TDR 2006
Purdue University

Plenary Lecture: Review of Geometrical and Interfacial Factors Determining the Effective Permittivity – Volumetric Water Content Relationships of Soils and Rocks

Schmulik P. Friedman (with S. B. Jones and D. A. Robinson)

Ref.: Friendman, Schmulik P., Jones, S. B. and Robinson, D. A., "Plenary Lecture: Review of Geometrical and Interfacial Factors Determining the Effective Permittivity – Volumetric Water Content Relationships of Soils and Rocks", Proc. TDR 2006, Purdue University, West Lafayette, USA, Sept. 2006, Paper ID 48, 21 p., https://engineering.purdue.edu/TDR/Papers

Review of Geometrical and Interfacial Factors Determining the Effective Permittivity –Volumetric Water Content Relationships of Soils and Rocks

S.P. Friedman[1], S.B. Jones[2], and D.A. Robinson[2,3]

[1] Institute of Soil, Water and Environmental Sciences (ARO), The Volcani Center, Bet Dagan 50250, Israel, vwsfried@agri.gov.il.

[2] Department of Plants Soils and Biometeorology, Utah State University, Logan UT 84322

[3] Department of Geophysics, Stanford University, 397 Panama Mall, Stanford CA 94305

Abstract

Understanding the relationship between the effective permittivity of soils and rocks and their porosity and volumetric water content is important because electromagnetic measurements are used to determine porosity and water content. In this lecture we are going to overview experimental and theoretical studies by other groups and ourselves aimed at improving our understanding of the way the geometrical and interfacial attributes of granular materials determine their effective permittivity. In order to avoid bound water and other interfacial effects when discussing the role of geometrical factors, we will refer to results obtained with coarse granular materials of low surface area, such as glass beads, quartz sand grains, tuff and mica particles. Measurements of the effective permittivity of anisotropic packings of mica particles and isotropic packings of glass beads, sand grains and tuff particles have demonstrated: 1) an alteration of the directional effective conductivities and permittivities of anisotropic packings attributed to particle shape and orientation; 2) a reduction in the permittivity of isotropic packings due to deviation from a spherical particle shape and an increased broadness of particle size distribution. The measured effective permittivities are predicted reasonably well by modified classical mixing formulas. Particle shape effects were modeled using the depolarization factors of equivalent oblate particles, and those of particle size distribution using a finite number of inclusion-intermediate background mixing. For dense granular packings of various particle shapes and size fractions of a background/inclusion permittivity ratio of 1/8 to 16, the effects of the neighboring particles can be accounted for with a single value, a = 0.2, of a heuristic parameter a defined in the range of 0 (Maxwell-Garnett / Clausius-Mossotti mixing law) to 1 (coherent potential approximation). Next we will discuss in brief two interfacial features affecting the effective permittivity of fine-textured soils: bound water and reduced near-surface water permittivity due to high ionic concentrations.

Key Words effective permittivity, soils, rocks, particle shape and size distribution, bound water

Introduction

In order to determine the volumetric water content (VWC, θ) from TDR measurements of the medium's effective permittivity (ε_{eff}), an ε_{eff} - θ calibration curve is required. In their seminal 1980[1]'s article, Topp et al. stated that this relationship is relatively universal for mineral soils, namely, that it does not change significantly from one soil type to another. The universal

calibration curve they provided (Equation 1), based on measurements made on 9 mineral soil samples is still the mostly widely used nowadays for translating permittivity readings to volumetric water contents, and this statement on the universal behavior was a significant factor for promoting the TDR method and making it a standard for in-situ water content determination.

$$\varepsilon_{eff} = 3.03 + 9.3\theta + 146\theta^2 - 76.7\theta^3 \qquad (1)$$

In addition to the empirical findings, there are also physical reasons for the universality of the ε_{eff} - θ relationships as compared to the relationships between the hydraulic, electrical, and thermal conductivities and the VWC (solute diffusivity is analogous to electrical conductivity). For the hydraulic and electrical conductivities, the only conducting phase is the aqueous phase, and the hydraulic conductivity depends also on the pore size squared. These cause a stronger dependence of the electrical and hydraulic conductivities on the VWC, and consequently, their dependence on the soil texture and structure is also stronger than the dependence of the soil effective permittivity (three solid-liquid-gaseous conducting phases and no particle/pore-size dependence) on these soil attributes. For the other diffusive transport property (no scale dependence), the thermal conductivity, the intrinsic conductivity ratios are approximately 5:1:0 for the solid-liquid-gas phases as compared to approximately 5:80:1 for the effective, 1-GHz permittivity; namely the solids are the dominant heat conductor, while the water is the dominant displacement electrical current conductor. Thus, the soil structure and texture (particle-particle contacts) affect the thermal conductivity – VWC relationship to a greater extent, and the large 5:80:1 conductivity contrast makes the 1GHz effective permittivity: 1) very sensitive to the VWC; and 2) less sensitive to the other soil and porous rock attributes, which sets the merits for determining water contents with TDR and other electromagnetic methods.

As stated above, for most TDR applications in coarse and medium-textured mineral soils Topp's universal ε_{eff}-θ calibration curve gives reasonably accurate water content determination. Nevertheless, along the years and with the spread of the TDR method in the last two and a half decades since Topp et al.'s seminal article[1],

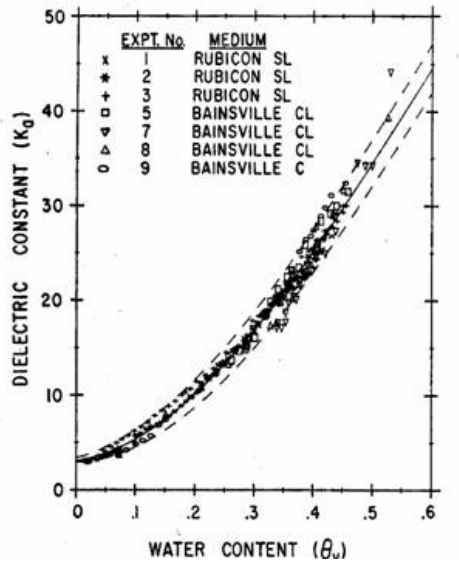

Fig. 1. The measured effective permittivities as a function of volumetric water content for four mineral soils varying in texture from sandy loam to heavy clay (symbols), the best-fitted universal function (solid line) and the confidence interval of ± 0.025 in θ (dashed lines) (From Topp et al., 1980[1]).

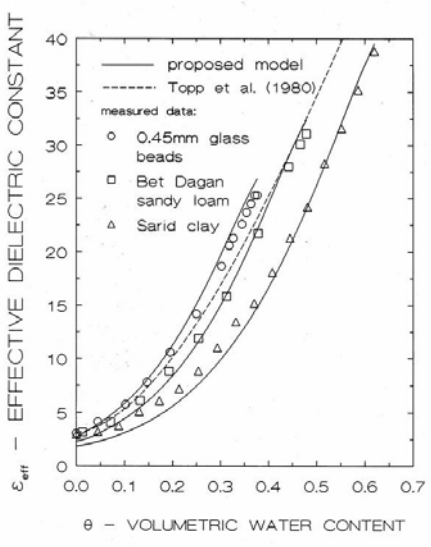

Fig. 2. The measured effective permittivities as a function of volumetric water content for three granular media (symbols), and their prediction according to the Friedman's (1998) [5] composite sphere model (solid lines). Also shown is the universal function of Topp et al., (1980) [1] (dashed line) (from Friedman (1998) [5]).

measurements of the ε_{eff}-θ relationships in more soils and other earth materials revealed differences among the various granular and porous media (Dobson et al., 1984[2]; Roth et al., 1992[3], Dirksen and Dasberg, 1993[4]; Friedman, 1998[5], See for example Figure 2).

In this lecture we will discuss the causes for these differences, namely the role of the various geometrical and interfacial soil attributes in determining the ε_{eff}-θ relationship. We will discuss first and in more detail the effect of geometrical attributes: particle shape and orientation and particle size distribution. Then we will discuss in brief the effects of bound water and elevated near-surface ionic concentrations on the 1GHz effective permittivity.

Geometrical Effects

1. Mean field theories – spherical particles

There are a few theoretical approaches for relating ε_{eff} of dielectric mixtures to their constituents' volumetric fractions and single-phase permittivities. Most of those fall into one of the two major conceptual categories of discrete capacitor network models (Ansoult et al., 1984[6]; Friedman, 1997[7]; Tabbagh et al., 2000[8]), which will not be discussed here, and continuum mean field theories. The latter category deals with the actual three-dimensional structure of the multiphase medium or with its idealized geometrical description. An evaluation of the real part of ε_{eff} involves solving the electrostatic problem, namely the Laplace equation for the electrical potential, while conserving the continuity of the potential and the normal displacement vectors on the interfaces between the various phases of different permittivities. In this respect, the mathematical and physical problem of the "static" effective permittivity is strictly analogous to the related conductive transport properties of magnetic permeability, electrical conductivity, thermal conductivity and diffusion coefficients. For real multiphase media such as wet soils and rocks, the Laplace equation can be solved by numerical methods, if their complex geometry can be reliably characterized and discretized. Another option is to refer to a simplified geometry of some common representative quantifiers, and to solve the electrostatic problem for the transformed medium. An exact analytical solution to the Laplace equation does not exist even for the most simplified mixture geometry one can conceive. Therefore, the common practice is to apply some approximating assumptions regarding the spatial structure of the electrical fields in the different phases, a concept which we will term here, mean field theories.

The three most common mean field theories are usually known in the context of the dielectric permittivity as the Maxwell-Garnett (1904) [9] and Polder-van Santen (1946) [10] models, and the coherent potential approximation (Tsang et al., 1985) [11]. The posed problem is that of finding a homogeneous material with an effective permittivity (ε_{eff}) equal to that of a mixture composed of similar size–dielectric spheres of permittivity ε_s, occupying a fraction f (=1-n) of the total volume, immersed randomly in a dielectric host of permittivity ε_0 and volumetric fraction n (porosity). The Maxwell-Garnett (1904) [9] formula (MG) is usually written in its explicit form for ε_{eff} as

$$\varepsilon_{eff} = \varepsilon_0 + 3(1-n)\varepsilon_0 \frac{\varepsilon_s - \varepsilon_0}{\varepsilon_s + 2\varepsilon_0 - (1-n)(\varepsilon_s - \varepsilon_0)} \qquad (2)$$

One pleasing feature of the MG mixing rule is its mathematical simplicity, explaining perhaps why it stems also from other kinds of argumentation (Sihvola, 1999[12]). It also provides the exact

ε_{eff} at the two end points of the background, $\varepsilon_{eff} = \varepsilon_0$, at vanishing inclusions ($n = 1$), and of the inclusions, $\varepsilon_{eff} = \varepsilon_S$, at complete filling ($n = 0$, which is actually impossible for monosize spheres). The geometric picture of approximately mono-size spheres randomly distributed in a host material is one of the simplest three-dimensional (3D) systems one can think of. The assumptions underlying the MG mixing formula are apparently over-simplified as well. Yet, surprisingly, the MG mixing model had proven to be a very good predicting tool for many two-phase mixtures [Hanai, 1968[13], Sihvola, 1999[12]], and even for water-saturated and oven-dried soils [Friedman, 1998[5]] and other granular materials [Robinson and Friedman, 2001[14], 2002[15], 2003[16]]. The MG prediction of e.g. $\varepsilon_{eff} = 35.6$ for $n = 0.5$, $\varepsilon_S = 5$ and $\varepsilon_W = 80$, is close to the value of $\varepsilon_{eff} = 34.6$, resulting from the common empirical relationship of Topp et al. (1980) [1] for a volumetric water content of 0.5. As opposed to it, the commonly used refractive index model (Birchack et al., 1974[17]; Whaley, 1993[18]) results in a much lower value of $\varepsilon_{eff} = 31.25$.

The other mean field theories can be presented via a universal mixing law (Sihvola and Kong, 1988[19], 1989[20]):

$$\varepsilon_{eff} = \varepsilon_0 + \left\{ \left[\frac{(1-n)(\varepsilon_s - \varepsilon_0)\left[\varepsilon_0 + a(\varepsilon_{eff} - \varepsilon_0)\right]}{3\left[\varepsilon_0 + a(\varepsilon_{eff} - \varepsilon_0) + (\varepsilon_s - \varepsilon_0)\right]} \right] \cdot \left[1 - \frac{(1-n)(\varepsilon_s - \varepsilon_0)}{3\left[\varepsilon_0 + a(\varepsilon_{eff} - \varepsilon_0) + (\varepsilon_s - \varepsilon_0)\right]} \right]^{-1} \right\} \quad (3)$$

containing a heuristic parameter, a, confined between 0 and 1, which accounts for the effect of neighboring particles on the internal electrical field of a reference particle. The universal model results in the MG formula when the value of a is 0, the symmetric effective medium approximation (Polder and van Santen, 1946[10]) (PVS) for $a = 2/3$ and the coherent potential (CP) mixing formula (Tsang et al., 1985[11]) when its value is 1. The permittivity $\varepsilon_a = \varepsilon_0 + a(\varepsilon_{eff} - \varepsilon_0)$ is in simple words that can be seen outside by the inclusion, and it can take different possible values from that of the host material, $\varepsilon_a = \varepsilon_0$, for the MG model up to the effective permittivity of the mixture, $\varepsilon_a = \varepsilon_{eff}$, for the coherent potential mixing rule. Among the classical three mixing formulas, the MG is probably the better predictor of the effective permittivity, at least for water (and other liquids)-saturated granular mixtures with $\varepsilon_s < \varepsilon_0$ (Robinson and Friedman, 2001[14], 2002[15], 2003[16]) and fused glass beads, representing sedimentary rocks (Sen et al., 1981[21]; Friedman, 1998). Yet, recently it was shown that letting $a = 0.2$ resulted in better prediction of the ε_{eff} of water-saturated packings of glass beads, sand grains and tuff particles (Friedman and Robinson, 2002[22], Figure 5 below), and also of glass beads immersed in liquids of different permittivity (Robinson and Friedman, 2005[23]).

2. Particle shape and orientation effects – anisotropic soils

Equation (3) applies to spherical solid particles, but the most important soil/rock attribute affecting its $\varepsilon_{eff}(n)$ relationship is probably particle shape, which varies from almost spherical sand grains to platy, disk-like clay tactoids. Some minerals appear also in long, needle-like form. It is practically impossible to calculate the effective permittivity of packings made of angular and rough-surfaces particles, and these features were also found secondary in affecting ε_{eff} (Friedman and Robinson, 2002[22]). Representing the particle geometry by an ellipsoid of revolution (spheroid) provides both: convenient analytical expressions and flexibility to be transformed into a number of shapes by altering the aspect ratio [Sihvola and Kong, 1988[19]; Sareni et al., 1997[24]; Jones and Friedman, 2000[25]]. By extending or contracting the b and c axes whilst

keeping *a* constant, a sphere can be transformed into either a disk-like (oblate) or needle-shaped (prolate) particle (Figure 3), as are often encountered in the natural environment. Particle shape is then incorporated in ε_{eff} modeling through a parameter named depolarization factor (N^i), which describes the extent to which the inclusion polarization is reduced according to its shape and orientation with respect to the applied electrical field. For the special cases of ellipsoids of revolution ($a \neq b = c$) Jones and Friedman (2000[25]) found that $N^a(a/b)$ can be approximated satisfactorily ($r^2 = 0.9999$) by a single empirical expression

$$N^a = \frac{1}{1+1.6(a/b)+0.4(a/b)^2} \quad ; \quad N^b = N^c = \tfrac{1}{2}(1-N^a) \qquad (4)$$

through the whole range of aspect ratio, *a/b*, from thin disks to long needles. The depolarization factors for a sphere where *a,b* and *c* are all equal in length are $N^{a,b,c}$ = ⅓, ⅓, ⅓, for a thin disk (extreme oblate): 1,0,0 and for a long needle (extreme prolate): 0, ½, ½.

Non-spherical particles can form either anisotropic or isotropic packings, depending on whether aligned in the same direction or randomly oriented. The effective permittivity of aligned, non-spherical particles, making a uniaxial–anisotropic medium, is not a scalar anymore, but a second order tensor, defined by its diagonal components $\varepsilon_{eff}^a \neq \varepsilon_{eff}^b = \varepsilon_{eff}^c$. The effective permittivity in the i[th] direction takes the form (Sihvola and Kong, 1988[19])

$$\varepsilon_{eff}^{\ i} = \varepsilon_0 + \frac{\dfrac{(1-n)[\varepsilon_0 + a(\varepsilon_{eff}^{\ i} - \varepsilon_0)](\varepsilon_s - \varepsilon_0)}{\varepsilon_0 + a(\varepsilon_{eff}^{\ i} - \varepsilon_0) + N^i(\varepsilon_s - \varepsilon_0)}}{1 - \dfrac{(1-n)N^i(\varepsilon_s - \varepsilon_0)}{\varepsilon_0 + a(\varepsilon_{eff}^{\ i} - \varepsilon_0) + N^i(\varepsilon_s - \varepsilon_0)}} \qquad (5)$$

(which reduces to Eq. (3) for spheres, $N^i = 1/3$) with the previously presented mixing parameter *a* accounting for the effect of neighboring particles on the internal electrical field, and the newly introduced depolarization factors (N^i), defined by the particle aspect ratio and alignment with respect to the applied electrical field. Knowing the effective permittvity in the principal anisotropy directions (ε_{eff}^a, ε_{eff}^b, ε_{eff}^c), the effective permittivity when the electrical field is directed arbitrarily, forming angles β^a, β^b, and β^c relative to the *a*, *b*, and *c*, coordinate axes, respectively, is given by

$$\varepsilon_{eff}^{\beta} = \varepsilon_{eff}^{a} \cos^2\beta^a + \varepsilon_{eff}^{b} \cos^2\beta^b + \varepsilon_{eff}^{c} \cos^2\beta^c \qquad (6)$$

Equations (5) and (6) can be used for demonstrating how the directional ε_{eff} parallel to the bedding plane of an oven-dried rock/soil ($\varepsilon_S = 5$, $\varepsilon_0 = \varepsilon_A = 1$, figure 3a) and water-saturated media ($\varepsilon_S = 5$, $\varepsilon_0 = \varepsilon_W = 80$, figure 3b) are larger than ε_{eff} of sphere packings, and the ε_{eff} perpendicular to the bedding plane smaller than the ε_{eff} of spheres, the effect being larger for oblate (disk-like) particles than for prolate (needle-like) particles of the same (reciprocal) aspect ratio. The calculated ε_{eff} are for anisotropic mixtures of a porosity of 0.5 with particles varying in shape from very thin disks (*a/b* = 0.001) through spheres (*a/b* =1) to very long needles (*a/b* = 1000). The CP mixing model is incompatible for the large dielectric contrast ($\varepsilon_0/\varepsilon_i = 16$) of a solid-water (SW) mixture. Arithmetic means of the phase permittivities ($\varepsilon_{SA} = 3$; $\varepsilon_{SW} = 42.5$) result from all three models for the ε_{eff}^b of "infinitely" thin disks (a/b = 0.001) and for the ε_{eff}^a of "infinitely" long needles (*a/b* = 1000). Harmonic mean permittivities result for MG and PVS models for ε_{eff}^a of thin disks (Figure 3a, $\varepsilon_{SA} = 1.67$; Figure 3b, $\varepsilon_{SW} = 9.41$). The MG model consistently predicts an effective permittivity closer to the background permittivity when compared to other mixing models. Needle-shaped particles produce unique permittivities perpendicular to their long axis (ε

$_{eff}^{b}$), which converges to a two dimensional circular problem. Considering the effect of particle shape with a sphere as reference, needles enhance ε_{eff}^{a}, measured along their long axis, due to the dipole resulting from their large length, and disks produce much lower permittivities perpendicular to their face ($\varepsilon_{\text{eff}}^{\text{a}}$) due to their large depolarizing influence (i.e., $N^a = 1$). In accordance, disks enhance $\varepsilon_{\text{eff}}^{b}$ more than that of spheres or needles due to the polarization resulting from the large disk diameter. Overall, the majority of the changes due to particle shape effects occur within an order of magnitude of the aspect ratio of a sphere ($0.1<a/b<10$), beyond which the shape effect on ε_{eff} changes little.

The above calculations of directional effective permittivities (Eq. 5) are for perfectly aligned spheroids. The particles forming real anisotropic media are, however, only partially aligned with respect to the principal anisotropy axes. The directional effective permittivities of such media can be calculated by using similar principles with the addition of the distribution of the particle's (long axis) orientation (Dafalias and Arulanandan, 1979[25]; Arulanandan, 1991[27]; Thevanayagam, 1993[28]).

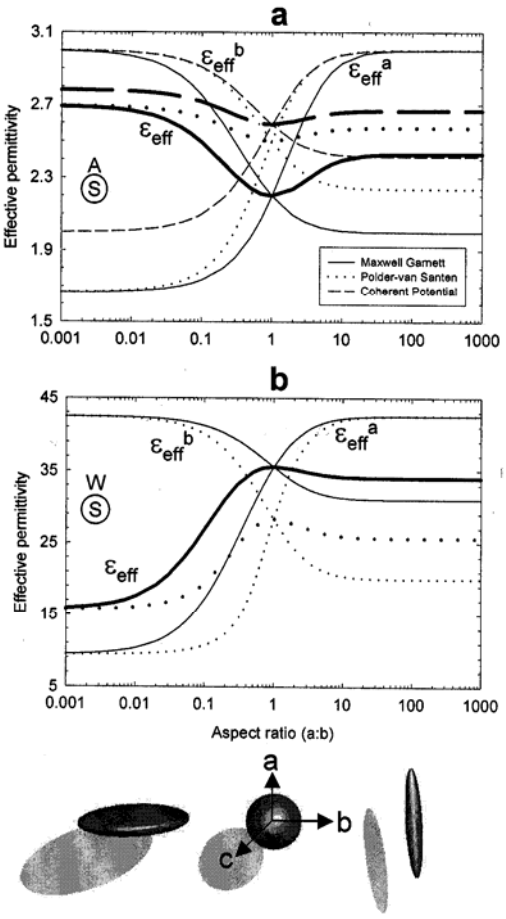

Fig. 3. Effective permittivity as a function of particle aspect ratio for two-phase mixtures of a) solids in air and b) solids in water, both having porosities of 0.5. Mixing models are according to line type with permittivities of aligned particles as indicated by ε_{eff}^{a} and ε_{eff}^{b}(thin lines), and bolded lines for ε_{eff}, the isotropic arrangement (from Jones and Friedman, 2000[25]).

To assess the effect of particle shape on the effective permittivity of unsaturated media, Jones and Friedman (2000[25]) used mica flakes, the $\varepsilon_{eff}^{a}(n)$ and $\varepsilon_{eff}^{b}(n)$ relationships of their water-saturated packings discussed above. The effective permittivity measurements were made using a couple of 3-wire TDR probes positioned in orthogonal directions in order to measure $\varepsilon_{eff}^{a}(\theta)$ and $\varepsilon_{eff}^{b}(\theta)$ relationships. For testing the experimental setup, Jones and Friedman (2000[25]) also measured the $\varepsilon_{eff}^{a}(\theta)$ and $\varepsilon_{eff}^{b}(\theta)$ of unsaturated packings of 0.5 mm glass beads, which are expected to be the same for the entire range of volumetric water content. Figure 4 (inset) shows the minimal impact which probe orientation had on horizontal and vertical permittivity measurements in the 0.5 mm glass beads. The observed small differences in horizontal and vertical measurements are likely a result of hydrostatic water distribution and its effect on the propagation of electromagnetic waves along the waveguides. The measured permittivities of the three different size fractions of mica particles are generally correlated to each other and to the electrical field alignment as determined by probe positioning (Figure 4). The modeling of the directional effective permittivities followed an extension of Friedman 1998[5]'s EMA mixing of two saturation degree-weighted solid-water-air (*SWA*) and air-solid-water (*ASW*) phase configurations (not discussed here). In their permittivity calculations, Jones and Friedman (2000[25]) used an average mica particles aspect ratio of 0.04, two different porosities of 0.7 to 0.8 and intrinsic dielectric constants of 6.35:78.5:1 for mica, water, and air.

The trend of higher effective permittivities in the direction of the bedding plane, $\varepsilon_{eff}^{b} > \varepsilon_{eff}^{a}$, is obvious, although the measured data generally lie between the ε_{eff}^{a} and ε_{eff}^{b} model predictions. The general gravitation of permittivity readings toward a central (isotropic) value between the predicted permittivities for the two principal directions is probably due to partial misalignment of the particles and due to excessive drainage of the horizontal pores adjacent to the vertically inserted TDR electrodes, which is highly correlated to particle size (i.e., most significant for ε_{eff}^{a} of 1 mm particles) and artificially decrease the readings of $\varepsilon_{eff}^{b}(\theta)$ (Friedman and Jones, 2001[29]). Data overall lie well below the Topp et al. (1980[1]) curve except for ε_{eff}^{b} values near saturation, while MG-based model predictions for ε_{eff}^{b} lie just above the Topp et al. curve.

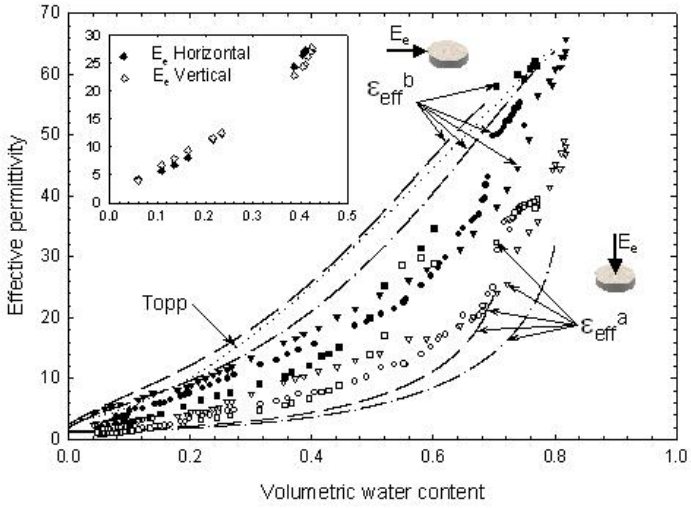

Fig. 4. Effective permittivity of three different mica flake diameters plotted as a function of water content. Particle sizes of 0.25, 0.5, and 1 mm are represented by triangles, circles and squares, respectively. Direction dependent measurements are indicated by ε_{eff}^{a} (empty symbols) and ε_{eff}^{b} (filled symbols). EMA model predictions for both electrical field alignments are shown for an aspect ratio of a/b = 0.04 and porosities of 0.7 (dashed line) and 0.8 (dash-dotted line). Inset figure shows the effects of probe orientation on permittivity measurements in an isotropic packing of 0.5 mm glass beads using the same probe configuration as in the mica (i.e., one horizontal and one vertical probe) (from Jones and Friedman (2000)[25]).

Assumptions and limitations of the proposed mixing model (Jones and Friedman 2000[25]) merit further discussion. The use of a single aspect ratio ellipsoidal geometry to model the mica flakes, and certainly soil particles, is of limited realism. Additionally, the elliptical water shells are not consistent with the water-air interface behavior except for very low water contents. Modeling the phases of solid, water, and air using a confocal arrangement, while mathematically efficient, does not ideally mimic the complex and variable configuration of partially saturated soils. Some of these discrepancies are partially corrected by the EMA mixing of the *SWA* and *ASW* phase configurations. In spite of the above limitations of the proposed model, and in light of the limitation of the experimental setup, we believe that the theoretical lines of Figure 4 are more representative of the real $\varepsilon_{eff}^{i}(\theta)$ relationships than the measurements. Particle shape effects are undoubtedly significant in determining the $\varepsilon_{eff}(\theta)$ relationship.

3. Particle shape effects – isotropic soils and rocks

Non-spherical particles, when oriented randomly, form an isotropic medium with a scalar effective permittivity, ε_{eff}. Applying a superposition principle, the isotropic version of the universal mixing law (Eq. 5) takes the form (Sihvola and Kong,1988[19])

$$\varepsilon_{eff} = \varepsilon_0 + \frac{\sum_{i=a,b,c} \frac{(1-n)[\varepsilon_0 + a(\varepsilon_{eff} - \varepsilon_0)](\varepsilon_s - \varepsilon_0)}{3[\varepsilon_0 + a(\varepsilon_{eff} - \varepsilon_0) + N^i(\varepsilon_s - \varepsilon_0)]}}{1 - \sum_{i=a,b,c} \frac{(1-n)N^i(\varepsilon_s - \varepsilon_0)}{3[\varepsilon_0 + a(\varepsilon_{eff} - \varepsilon_0) + N^i(\varepsilon_s - \varepsilon_0)]}} \quad (7)$$

Figure 3 demonstrates also particle shape effects on the ε_{eff} of 5:1 (a, oven-dried) and 5:80 (b, water-saturated) isotropic mixtures of porosity of 0.5, made of randomly oriented particles, varying in shape from very thin disks through spheres to very long needles. The effect of particle shape is again larger for disk-shaped particles than for needle-shaped, when compared to spheres. This effect arises from the large depolarization of disk-shaped particles and the accompanying attenuation of the electrical field, producing mixture effective permittivities closer to the inclusion permittivity. The CP solution fails again when the difference between background and inclusion permittivity is large ($\varepsilon_0/\varepsilon_i$ = 16). Realistically, disks (and needles) are not likely to be oriented randomly in natural environments, and would also pose much larger porosities than spherical particles (Jones and Friedman 2000[25]), resulting in mixture permittivities closer to that of the background on this respect.

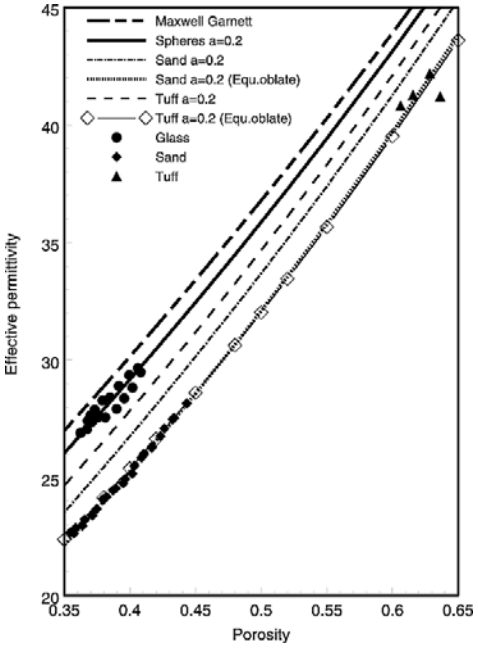

Fig. 5. Effective permittivity as a function of porosity for glass beads (ε_S = 7.6), quartz sand (ε_S = 4.7) and tuff grains (ε_S = 6.0). Predictions of permittivity are presented for equivalent oblates of a/b = 0.465 for sand and 0.364 for tuff. Note that the sand and tuff lie on lines close together due to the difference in the permittivity of the solid grains (from Friedman and Robinson, 2002[22]).

In spite of the expected significant particle shape effects demonstrated above, it is as difficult to incorporate the effect in practical $n(\varepsilon_{eff})$ and $\theta(\varepsilon_{eff})$ determinations as it is to quantify the 'average' shape characteristics of earth materials. Therefore, a method which would capture the three-dimensional shape characteristics of a granular material in regards to its packing geometry would be of great interest. In a recent attempt Friedman and Robinson (2002[22]) examined the use of measuring the angle of repose and the maximum angle of stability of a slope of poured granular material as a simple and rapid method of quantifying an 'effective' particle shape factor. They found high correlations between slope angles and a shape factor ($4\pi Area/Perimeter^2$, changing from 0 for a very non-spherical particle to 1 for a sphere), determined by image analysis of two-dimensional particle micrographs, and proposed to use the easily-measurable slope angles for routine particle shape characterization, because of their simplicity and also because of their beneficial sensitivity to surface roughness and particle angularity effects beyond the aspect ratio of a smooth equivalent ellipsoid. As already mentioned above, best-fitting equation (7) to the measured ε_{eff} of the water-saturated glass spheres (a/b =1) at different porosities resulted in a mixing value parameter of a = 0.2, slightly higher than Maxwell-Garnett's a = 0, which constitutes as expected an upper bound for the measured ε_{eff} (Figure 5). Friedman and Robinson (2002[22]) calculated the aspect ratios of oblate particles equivalent to the sand (a/b = 0.465) and tuff (a/b = 0.364) grains, giving the same shape factors as those correlated to their measured

maximum angle of stability. These aspect ratios and the previously determined solid permittivities were used to predict the $\varepsilon_{eff}(n)$ relationships of their packings, with the help of Equation (7), while fixing the heuristic mixing parameter at $a = 0.2$ (for relatively low a values, close to the MG mixing mode, a is not expected to be considerably dependent on the particle shape). The agreement between the measured and predicted $\varepsilon_{eff}(n)$ relationships of the packings of the non-spherical sand and tuff particles is remarkable (Figure 5). Lines are also presented for the predicted ε_{eff} using $a = 0.2$, but with the depolarization factors set for spheres ($N^{a,b,c} = {}^1/_3, {}^1/_3, {}^1/_3$). It is clearly observed that the use of the depolarization factors (obtained from the slope measurements) greatly improves the prediction.

To summarize particle shape effects on the $\varepsilon_{eff}(\theta)$ relationship: near water saturation non-spherical soil and rock particles can decrease $\varepsilon_{eff}(n)$ substantially by up to 20%, whereas, at complete dryness $\varepsilon_{eff}(n)$can be higher by up to 10% as compared to spherical particles of same permittivity, packed to similar porosities. The reversal point, where particle shape is not expected to affect the $\varepsilon_{eff}(\theta)$ relationship, is at relatively small saturation degrees.

3. Particles size distribution

In the previous theoretical computations, the particles comprising the medium were assumed to be of similar size when deriving and applying the mixing models. As the effective permittivity does not include any length dimension, it does not depend on the absolute particles size, which was not addressed directly. Yet, when mixing particles of differing size, the better conducting paths are expected to be more tortuous, which should affect also the medium's effective permittivity (Guyon et al., 1987[30]; Robinson and Friedman 2001[14]). The first trivial effect of mixing, e.g., large and small spherical particles, is a reduction of porosity as compared to the mono-size packings, which should reduce also the effective permittivity in the case of $\varepsilon_0 > \varepsilon_i$ (water-saturated soils). The problem addressed by Robinson and Friedman (2001[14]) and discussed here is the effect of increasing width of the particle size distribution on the $\varepsilon_{eff}(n)$ relationship beyond the porosity reduction. To model the effective permittivity of a binary mixture of substantially differing-in-size large and small spheres, Robinson and Friedman (2001[14]) propose a two-mixing-step approach: First, the smaller particles of permittivity ε_1 and volumetric fraction f_1 are being mixed into the background of ε_0 and volumetric fraction n (porosity) with e.g. the MG equation for spherical particles (2) to obtain an effective permittivity ε_B for this intermediate mixture

$$\varepsilon_B = \varepsilon_0 + 3\left(\frac{f_1}{n+f_1}\right)\varepsilon_0\left(\frac{\varepsilon_1-\varepsilon_0}{\varepsilon_1+2\varepsilon_0-\left(\frac{f_1}{n+f_1}\right)(\varepsilon_1-\varepsilon_0)}\right) \qquad (9)$$

Then they treat ε_B as the background and mix the large spheres of ε_2 and f_2 into the intermediate ε_B background to get

$$\varepsilon_{eff} = \varepsilon_B + 3f_2\varepsilon_B\left(\frac{\varepsilon_2-\varepsilon_B}{\varepsilon_2+2\varepsilon_B-f_2(\varepsilon_2-\varepsilon_B)}\right) \qquad (10)$$

As a result, an incremental mixing is developed based on the number of size fractions present, m,

to give the value of the final effective permittivity of the mixture, the general equation being:

$$\varepsilon_{eff} = \varepsilon_{B(m-1)} + 3 f_m \varepsilon_{B(m-1)} \left(\frac{\varepsilon_m - \varepsilon_{B(m-1)}}{\varepsilon_m + 2\varepsilon_{B(m-1)} - f_m(\varepsilon_m - \varepsilon_{B(m-1)})} \right) \qquad (11)$$

Repeating the recursive mixing procedure endlessly for the case of spheres with a single solid permittivity (ε_1) results in an effective permittivity equal to that predicted by the model of Sen et al. (1981[21]), derived for a self-similar medium of infinitely wide particle size distribution

$$\left(\frac{\varepsilon_1 - \varepsilon_{eff}}{\varepsilon_1 - \varepsilon_0} \right) \left(\frac{\varepsilon_0}{\varepsilon_{eff}} \right)^{1/3} = n \qquad (12)$$

These two mixing models, Maxwell-Garnett for mono-size spheres (2) and that of Sen et al. (1981[21]), should therefore form the upper and lower bounds for real water-saturated ($\varepsilon_0 > \varepsilon_i$) granular materials of bounded particle size distribution, with changing roles for the opposite, air-dried case ($\varepsilon_0 > \varepsilon_i$). This is indeed observed in Figure 6 (left), presenting TDR measurements of the $\varepsilon_{eff}(n)$ relationship of water-saturated binary mixtures of different fractions of small glass spheres (45-53μm) mixed into larger ones (450-500μm) of similar solid permittivity. The lines represent the predicted effective permittivity according to the MG model (2) and the Sen et al. (1981[21]) self similar model (12) for a solid with a permittivity of ε_S = 6.75 immersed in water with a permittivity of ε_W = 78.5, forming the expected upper and lower bounds to the measurements. The Maxwell Garnett model is plotted down to a minimal porosity of 0.26, representing the porosity of a face-centered cubic packing of monosize spheres. A value of 0.35 was found to be the minimum achievable porosity using monosize beads. As the mixing of small beads into large occurs, so the data can be seen to diverge from the MG prediction towards that of Sen et al. (1981[21]), and converge back to the MG prediction as the mixing progresses to monosize small beads. The prediction of the two-step mixing model (9, 10), represented by a cross for each of the seven data sets and connected with cubic splines, follows the pattern of the data, lying slightly above the measured values, which is a very acceptable agreement, considering the inherent experimental difficulties. Using similar binary mixtures of small and large quartz sand grains immersed in water, Robinson and Friedman (2001[14]) got similar results with lower $\varepsilon_{eff}(n)$ relationships because of the non-spherical particle shape (Figure 6, right plate).

As another step towards a continuous particle size distribution, Robinson and Friedman (2001[14]) also conducted measurements in quartic mixtures made of four size fractions of water-saturated glass beads. Three mixtures were used with mass fractions of 0.1,0.2,0.3,0.4; 0.4,0.3,0.2,0.1; 0.25,0.25,0.25,0.25 for the (45-53 μm), (90-106 μm), (180-212 μm) and (450-500 μm) beads, respectively (Figure 6, middle plate). The three mixtures represent uniform (solid spheres), increasing (solid triangles), and decreasing (empty triangles) particle size distributions. Again, the Maxwell Garnett and Sen et al. models provide upper and lower bounds (the data for the monosize spheres are the same as presented in Figure 6, left plate). All three mixtures show the reduction in the effective permittivity compared to monosize packing. The predictions of the four step mixing (Eq. 11, m = 4) are in remarkably good agreement with the data.

It should be noted that the observation of the data for both small and large monosize spheres packed to different porosities following the line predicted by the Maxwell Garnett model (2) (Figure 6), stems probably from the too low evaluation of the glass spheres permittivity, ε_S = 6.75. The later ε_S determination of Robinson and Friedman (2003[16]) to be 7.6 is most likely

more realistic, and using this value with the MG mixing model (2) would result in the expected upper bound to the measured $\varepsilon_{eff}(n)$ data. One should also bear in mind that the binary system of 50 and 500 μm glass spheres referred to in that study is quite different from the sand-clay mixtures of natural soils, since the clay particles are non-spherical and usually smaller than the sand grains, by a factor much greater than 10. Soil clay particles usually form into aggregated (flocculated) states, rather than having been single particles, and also initiate bound water effects, seriously reducing the permittivity of the water in contact with the clay plates. Therefore, one should not directly infer from the results of Robinson and Friedman's (2001[14]) study to mixtures of sand, silt and clay particles constituting real soils.

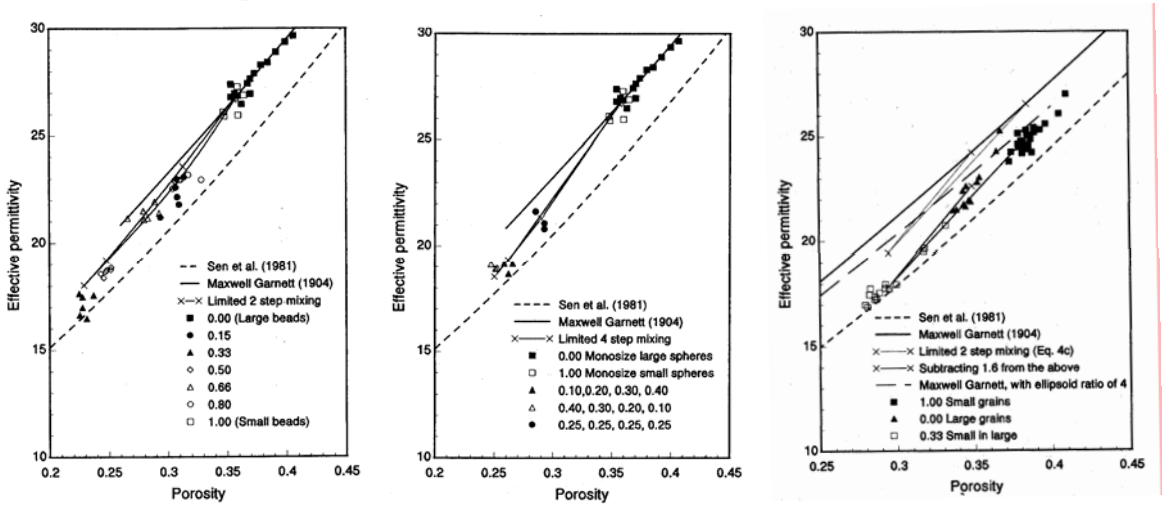

Fig. 6. Measurements of the effective permittivity of binary mixtures of glass beads (left) and quartz sand grains (right) at saturation and the predictions by the Maxwell Garnett (2) and Sen et al (12) models and the presented two-step mixing method. The middle chart presents measurements of quartic mixtures of glass beads at saturation and the predictions with a four step mixing (Eq. 11, $m = 4$) (from Robinson and Friedman (2001[14])).

The low effective permittivities of air-dried samples cannot be measured accurately with the TDR method, and Robinson and Friedman (2001[14]) used equations (9) and (10) to evaluate the expected increase in the $\varepsilon_{eff}(n)$ relationship of small-large spheres mixtures in the porosity range of 0.2 to 0.5, as compared to mono-size dry packings. The calculated relative increase in effective permittivity for e.g. ¼ oven-dry small spheres mixed into ¾ large ones and a porosity of 0.4, was of 3%, and the relative decrease in the effective permittivity of such water-saturated binary mixture was 7%. Thus, the expected effect of particle size distribution in the relationships is relatively limited and can be disregarded.

In the lecture, we are going to discuss in brief other related issues also, such as the permittivity of multi-shape particle mixtures (Jones, unpublished), the effects of the solid phase permittivity (Robinson and Friedman, 2002[15],2003[16], Robinson, 2004[31]), aggregation (Miyamoto et al., 2005[32]; Blonquist Jr. et al., 2006[33]), and also present some measurements and computations of the effective (apparent) electrical conductivity of the same coarse-textured media (Friedman and Jones, 2001[29]; Friedman, 2005[34]).

Interfacial Effects

1. Bound Water

The presence of soil minerals affects the dielectric properties of the water molecules adjacent to their surfaces by restricting their rotational movements, thus reducing their polarizability and permittivity, as compared to that of free water at the same temperature and frequency. Dirksen and Dasberg (1993[4]) assumed that the soil minerals are surrounded by a single monomolecular layer of bound water of a MHz-GHz permittivity of 3.2, as that of ice, and that the rest of water is free water. Friedman (1998[5]) adopted a slightly more detailed pragmatic approach and assumed that the MHz-GHz permittivities of bound water grow in an exponential mode with the distance from the solid surface, x, from their minimal value at $x = 0$ (ε_{min}) to the maximum value of free water (at the given temperature, frequency and solute concentration, ε_{max}), according to a general scaling length, $1/\lambda$, common to all soil minerals:

$$\varepsilon = \varepsilon_{\min} + (\varepsilon_{\max} - \varepsilon_{\min})(1 - e^{-\lambda x}) \quad ; \; \varepsilon_{\min} = 5.5 \; ; \lambda = 10^8 \text{ cm}^{-1} \qquad (13)$$

This $\varepsilon(x)$ relationship is an upper bound to some published estimations for ε near interfaces, *e.g.*, 41 for the first monolayer of water vapors adsorbed on silica gel and 66 for the second monolayer (Thorp, 1959[35]), and 6, 32 and 80 for the first, second and third molecular layers for water near metal surfaces (Bockris et al., 1963[36]) (Figure 7). Friedman (1998[5]) has used this upper bound for $\varepsilon(x)$; as for the average water-phase permittivity (ε_W), he took the harmonic mean of $\varepsilon(x)$, which is a lower estimate for ε_W. Robinson et al. (2002[37]) assumed a lower exponential $\varepsilon(x)$ relationship for the bound water:

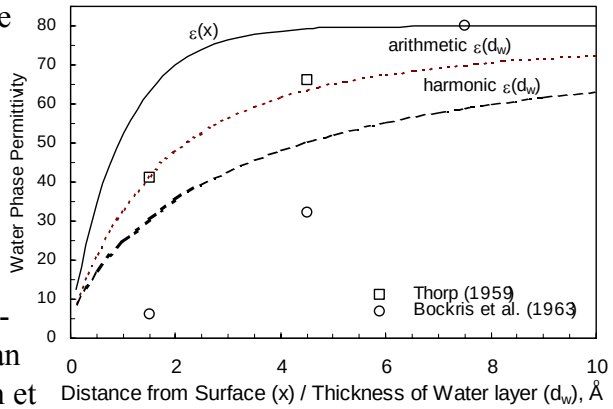

Fig. 7. The water phase permittivity as a function of the distance form the solid surface and its arithmetic and harmonic means (after Friedman (1998[5])).

$$\varepsilon = \varepsilon_{\max}\left(1 - e^{-\frac{1}{\beta}x}\right) \quad ; \quad \beta = 0.28 \text{ nm} \qquad (14)$$

starting with a zero permittivity on the mineral surface and increasing according to a scaling length of $\beta = 0.28$ nm, the diameter of a water molecule, as compared to 0.1 nm of Eq. (13). They also suggested that the amount of 0.28 nm thick-assumed bound water be equivalent to the easily measurable hygroscopic water content of the soil, in agreement with the high correlation between the amount of hygroscopic water at 50% relative humidity and a single monomolecular layer found by Dirksen and Dasberg (1993[4]).

According to the classical Debye (1929[38]) model the dielectric relaxation time of liquids is directly related to their viscosity

$$\tau = \frac{4\pi r^3}{k}\frac{\eta}{T} \qquad (15)$$

(r–the radius of the molecule, k – Boltzmann's constant (1.38 x 10^{-23} J/molecule·ºK), η – dynamic viscosity, T– absolute temperature (ºK)), which appears to hold almost exactly for free

water (Grant, 1957[39]; Kaatz, 1996[40]). It is also known that the viscosity of interlayer water increases exponentially towards the clay surfaces (Low, 1976[41]; McBride and Baveye, 1995[42]). Or and Wraith (1999)[43] had utilized these two relationships to derive a physically-based relationship for the dielectric relaxation time as a function of x. They modified Low's (1976) [41] viscosity-distance expression to be:

$$\eta(x,T) = \eta_o(T)e^{\frac{a}{xT}} \qquad (16)$$

where $\eta_0(T)$ is the temperature dependent viscosity of bulk water, represented as $\eta_0(T) = c\cdot\exp(d/T)$ (c = 9.5 Pa·s, d = 2047 Kº), and a = 1621 Å·ºK, and after substituting it in the Debye model (Eq. 15) received for the relaxation frequency (Or and Wraith, 1999[43]):

$$f_{rel} = \frac{1}{2\pi\tau} = \frac{kTe^{-\frac{1}{T}\left(\frac{a}{x}+d\right)}}{8\pi^2 r^3 c} \qquad (17)$$

Or and Wraith (1999[43]) suggested to use a rather larger molecular radius of 2.5 Å because of higher, average macroscopic relaxation times (as compared to the single molecule τ) and the participation of water molecules in the cation hydration shells. Here, the conservative radius of 1.44 Å (Sposito, 1981[44]), giving the $\tau(T)$ relationships for free water (Figure 8) as $x \rightarrow \infty$, is used for demonstrating the effect of the solid surfaces on reducing the relaxation frequencies at the different temperatures (Figure 8). For modeling purposes, Or and Wraith (1999[43]) proposed to characterize the bound water as a single layer with a temperature-independent permittivity of 12 and thickness determined by letting the relaxation frequencies of its water molecules be lower than a cut-off frequency of the measuring device (e.g., 1GHz for a Tektronix 1502B cable tester), $x(f_{rel}, T)$ from Eq. (17).

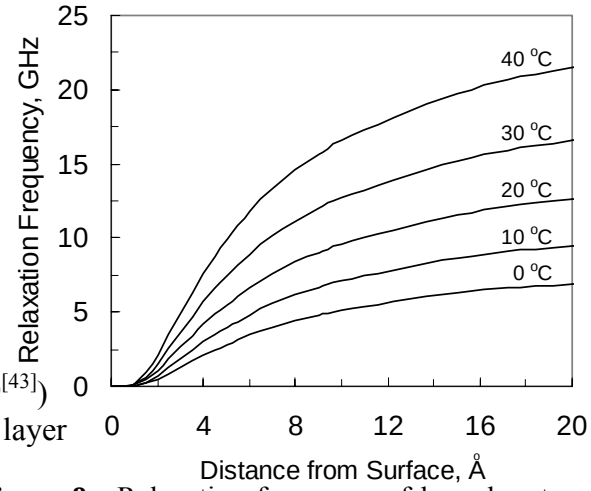

Figure 8. Relaxation frequency of bound water as a function of the distance from the solid surface (after Or and Wraith (1999[43])).

The above studies related the properties of the bound water, e.g., their relaxation frequency, to the distance from the mineral surfaces. An alternative thermodynamic approach had been proposed recently by Hilhorst et al. (2001[45]), suggesting to relate the relaxation frequency to the activation enthalpy of the water, which is related in turn to the water matric potential in the soil. The relaxation frequency should be related, in principle, to the change in the Gibb's free energy required to break the hydrogen bonds ($\Delta G^* = \Delta H^* - T\Delta S^*$), but since the activation entropy (ΔS^*) is approximately independent of the binding forces, the relaxation frequency can be related solely to the activation enthalpy (ΔH^*) (Hilhorst et al.,2001[45]):

$$f_{rel} = \frac{kT}{2\pi h} e^{\frac{\Delta H^*}{RT}} \qquad (18)$$

where h is Planck's constant (6.63 x 10^{-34} J/s) and R the universal gas constant (8.314 J/mol· ºK). The ratio between the relaxation frequencies of bound and free water (e.g., at atmospheric pressure, 20ºC) is accordingly

$$\frac{f_{rel}^{bw}}{f_{rel}^{fw}} = \frac{\Delta H_{fw}^{*} - \Delta H_{bw}^{*}}{\mathrm{RT}} \qquad (19)$$

Then, Hilhorst et al. (2001[45]) claim that the difference in the free and bound water activation enthalpies can be related to the soil matric pressure p_m (Pa) (and molar volume of the water, V (m^3/mol))

$$\frac{f_{rel}^{bw}}{f_{rel}^{fw}} = e^{\frac{p_m V}{\mathrm{RT}}} \qquad (20)$$

The activation enthalpy of free water is about 20.5 kJ/mol at 20ºC, and it increases significantly, e.g., to 22.3 kJ/mol, only when the matric pressure decreases down to -100 MPa (related to a monomolecular layer in equilibrium with 50% relative humidity), which corresponds to a decrease in the dielectric relaxation frequency from 17 to 8 GHz (Hilhorst et al., 2001[45]). This demonstrates the limitation of this macroscopic thermodynamic approach to characterize the dielectric properties of the water. While at practical soil water matric pressures of -100 MPa (-1000 atmospheres) and higher (less negative), corresponding relaxation frequencies converge quickly to that of free water (according to Eq. 20). The first molecular layers adjacent to the mineral surfaces still experience their binding forces, and their dielectric reorientation is restricted. In fine-textured soils, these bound waters constitute a significant fraction of the soil water in the whole range of water contents, and the matric pressure in Eq. (20) is irrelevant for characterizing their relaxation properties. Therefore, for wet soils at matric pressures more positive than -1 MPa, the relaxation frequencies were found to be in the 100MHz-1GHz frequency range (Hoekstra and Delaney, 1974[46]; Friel and Or, 1999[47]; Shang et al., 1999[48]), much below that of free water.

After discussing the dielectric properties of water bound to surfaces in general and in particular to the soil minerals, we are ready to discuss how bound water can be incorporated into mixing models, and to demonstrate their expected effects on the $\varepsilon_{eff}(\theta)$ relationships of fine-textured materials. For these purposes, we will use the expression proposed by Friedman (1998[5]) to describe the frequency-independent-assumed $\varepsilon(x)$ function (water permittivity – distance from mineral surface, equation (13)). This expression, which seems to form an upper bound to some measured values (Figure 10), was chosen. As for the average permittivity of the water phase, a layer of thickness d_w surrounding the solid particles, Friedman (1998[5]) took the harmonic mean of Eq. (13)

$$\frac{1}{\varepsilon_W} = \frac{1}{d_w}\int_0^{d_w} \frac{1}{\varepsilon(x)}\,dx \qquad (21)$$

which is a lower bound to the water-phase permittivity, resulting in

$$\varepsilon_W(d_w) = \frac{d_w \varepsilon_{\max}}{d_w + \frac{1}{\lambda}\ln\left[\frac{\varepsilon_{\max} - (\varepsilon_{\max} - \varepsilon_{\min})e^{-\lambda d_w}}{\varepsilon_{\min}}\right]} \qquad (22)$$

with $\lambda = 10^8$ cm^{-1}, $\varepsilon_{min} = 5.5$ and ε_{max} describing the free water permittivity. The average thickness of the water shell, d_w, can be calculated by dividing the volume of water contained in a volume of the bulk soil by the wettable surface areas of its solid phase, which for a unit soil volume, means dividing the volumetric water content by the product of the soil bulk density, ρ_b (ML^{-3}), and specific surface area, S_{SA} (L^2M^{-1})

$$d_w = \frac{\theta}{\rho_b S_{SA}} \qquad (23)$$

This approach was adopted by other researchers, e.g., Cosenza et al. (2003[49]).

In principle, the varying permittivity of water as a function of the distance from the solid phase can be treated by adding shells of differing ε_{Wi} to a multi-layered composite inclusion, followed by applying the mathematically more complex expressions of Sihvola and Lindell (1990[50]) for the resulting effective permittivities. Another possibility is to add just another single fourth phase of permittivity ε_{BW} most suitably located in between the solid and free water phases. Yet, because of the other simplifying assumptions involved and the desire to simplify the calculation procedure, the treatment as a single shell of water with a permittivity $\varepsilon_W \neq 80$ was preferred by Friedman (1998[5]) and Jones and Friedman (2000[25]). The curvature of the water shell was also ignored in evaluating $\varepsilon_W(d_W)$, as implied from equation (22).

The above analysis refers to a water shell of constant thickness d_w, as if it was spread on a flat surface, ignoring also the particle shape effect in the sense that ellipsoidal particles have larger surface areas than spherical particles of the same volume. The combined effects of bound water and particle shape were also analyzed by Jones and Friedman (2000[25]), using (22) and (23) with $\lambda = 10^8$ cm^{-1}, $\varepsilon_{min} = 5.5$ and $\varepsilon_{max} = 80$. Their $\varepsilon_{eff}(\theta)$ calculations with surface area-dependent estimates of bound water particle fortify the statement made above that shape effects play a significant role in altering the effective permittivity of fine-textured soils, which usually contain primary and secondary particles, which are both non-spherical and sub-micrometer-sized.

2. Reduced near-surface water permittivity due to high ionic concentrations

One reason for reduced water permittivity in fine-textured soils is the direct interaction between water molecules and solid surfaces, inhibiting their polarization and decreasing their relaxation frequency, as discussed above. Another reason which has not been given enough attention is the effect of high ionic concentration near mineral and organic matter surfaces. Part of the compensating (for the negatively charged soil particles) excess cations are tightly adsorbed on the solid surfaces (Stern layer), and the binding energy of the others comprising the diffuse part of the double layer (the Gouy layer) is relatively low, few kJ/mole (Li and Friedman, 2005[51]), and they easily undergo exchange processes. The counterion concentration can be as high as a few moles/l, as demonstrated, e.g., in the theoretical computations presented in Figure 9. For a charge density of 0.146C/m^2 and a background ionic strength of 0.01M, the surface cation concentration is expected to rise by a factor of 500, namely to 5M.

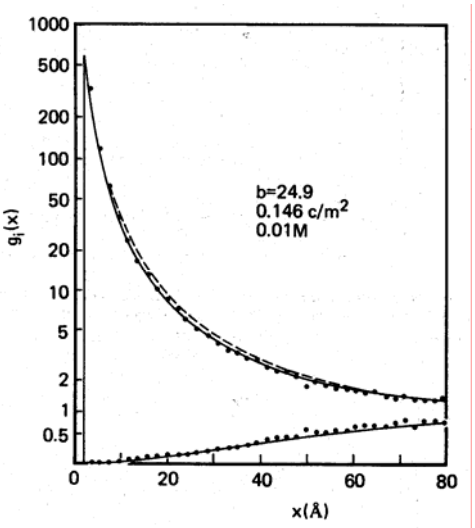

Fig. 9. Ionic distribution functions of a 0.01M model monovalent ionic fluid (σ=4.25Å-ionic diameter, T=298K, ε=78.5). The points are computer simulation results, and broken and solid curves the classical Gouy-Chapman theory and the Hypernetted Chain-mean Spherical Approximation results, respectively. From Henderson (1983[52]).

At such elevated ionic strengths, the water permittivity is significantly reduced, depending also on the electrolyte

type. All three Debye parameters, ε_0, ε_{inf} and τ, are affected by the presence of solutes; the more significant effect in the 100MHz-1GHz frequency range is on the static permittivity, ε_0. Figure 10 presents the measured static permittivities of LiCl and KCl solutions, showing ε_0 - drops of 13% and 17% compared to distilled water (78.3 at 25ºC) at the maximal concentration of 1 mol/l. At further high concentrations, $\varepsilon_0 \varepsilon_0$ continues to decrease to e.g. ε_0 = 21 for 14 mol/l LiCl (Pottel, 1973[53]). It is true that the usual ionic strengths of natural and irrigated soil solutions is up to about 0.1 M for which the electrolyte effect, 2% drop in ε_0, can be regarded negligible, but as demonstrated above (Figure 9) in the diffuse double layer (DDL) near the soil minerals, the cation concentrations can exceed 1M and the permittivity reduction can be significant. The mechanism by which the electrolytes reduce the static permittivity is the formation of hydrated shells of water molecules around the ions, these molecules exhibiting restricted orientational polarizability. The number of non-polarizable hydrated water molecules is determined by the surface charge density on the cation, and therefore, it is maximal for the smaller ion, Li^+. Divalent cations interact with more non-polarizable water molecules, e.g., about 12 for Ca^{2+}, and therefore reduce the static permittivity more significantly. The effect of the anion type is less pronounced (in contrast, the permittivity reduction is greater for the larger anions), and their near surface concentrations are negligible (Figure 9). The ionic permittivity reduction is similar for the temperature range of 0 to 50ºC, as demonstrated for 1M NaCl compared to distilled water in Figure 11. For most simple electrolytes, the relaxation time, τ, decreases with increasing ionic strengths. An example of this decrease for 1M NaCl is given in figure 11, where it can be seen that the drop in τ is maximal at 0ºC and diminishes with increasing temperatures. For some electrolytes the ionic effect on the dielectric relaxation time is more complex and sometimes opposite of increasing relaxations times. High frequency permittivity, ε_{inf}, tends to increase with increasing ionic strengths, but this effect is insignificant when referring to the MHz-GHz water permittivities.

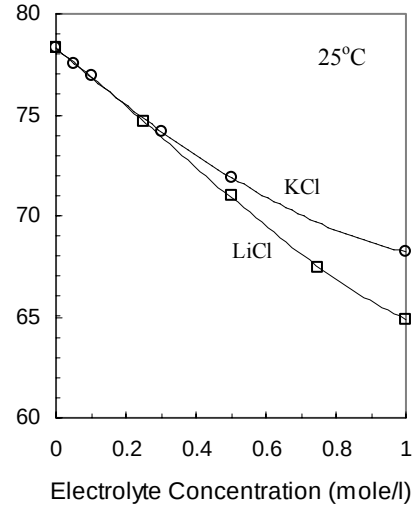

Fig. 10. Measured static permittivities of LiCl and KCl solutions of different concentrations (data form Pottel (1973[53]).

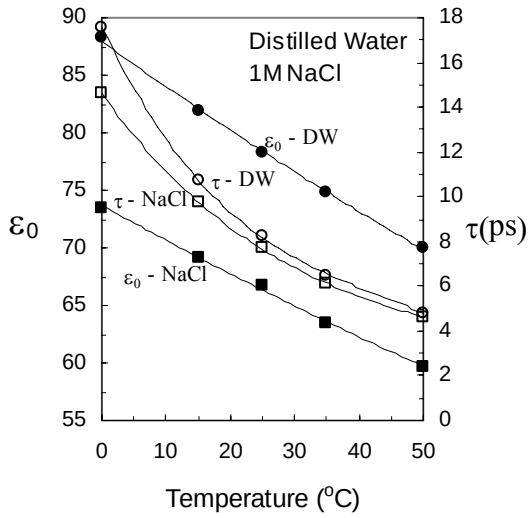

Fig. 11. The temperature dependence of the static permittivity and relaxation time for 1M NaCl solution compared to that for distilled water (data from Pottel (1973[53]).

In the lecture we are also going to briefly discuss potential Maxwell-Wagner relaxation effects on soil effective permittivity (Chen and Or, 2006[54]).

Acknowledgments

The authors wish to acknowledge the funding provided for this project from the BARD, the United States - Israel Binational Agricultural Research and Development Fund (Project no. IS-2839-97).

References

[1] Topp, G. C., J. L. Davis, and A. P. Annan (1980). Electromagnetic determination of soil water content: Measurements in coaxial transmission lines, *Water Resour. Res.*, *16*, 574-582.

[2] Dobson, M. C., F. Kouyate, and F. T. Ulaby (1984). A reexamination of soil textural effects on microwave emission and backscattering, *IEEE Trans. Geosc. Remote Sensing, GE-22*, 530-536.

[3] Roth, C. H., M. A. Malicki, and R. Plagge (1992). Empirical evaluation of the relationship between soil dielectric constant and volumetric water content as the basis for calibrating soil moisture measurements by TDR, *J. Soil Sci., 43*,1-13.

[4] Dirksen, C., and S. Dasberg (1993). Improved calibration of time domain reflectometry soil water content measurements, *Soil Sci. Soc. Am. J., 57*, 660-667.

[5] Friedman S. P. (1998). A saturation degree-dependent composite spheres model for describing the effective dielectric constant of unsaturated porous media. *Water Res. Research*., *34*, 2949-2961.

[6] Ansoult, M., L. W. De Backer, and M. Declercq (1985). Statistical relationship between apparent dielectric constant and water content in porous media, *Soil. Sci. Soc. Am. J., 49*, 47-50.

[7] Friedman, S. P. (1987). Statistical mixing model for the apparent dielectric constant of unsaturated porous media, *Soil Sci. Soc. Am. J.*, *61*, 742-745.

[8] Tabbagh, A., Camerlynk, C., and P. Cosenza (2000). Numerical modeling for investigating the physical meaning of the relationship between relative dielectric permittivity and water content of soils, *Water Resour. Res.*, *36*, 2771-2776.

[9] Maxwell-Garnett, J. C. (1904). Colours in metal glasses and in metal films, *Trans. R. Soc. London*, *203*, 385-420.

[10] Polder, D., and J.H.V. Santen (1946). The effective permeability of mixtures of solids. *Physica* XII:257-271.

[11] Tsang, L., Kong, J.A., Shin, R.T. (1985). *Theory of Microwave Remote Sensing.* John Wiley, New York.

[12] Sihvola, A. (1999). *Electromagnetic mixing formulas and applications.* IEE Electromagnetic Waves Series No. 47., Institution of Electrical Engineers, Stevenage, Herts., UK.

[13] Hanai, T. (1968). Chap. 5. Electrical Properties of Emulsions. pp. 353-478, In *Emulsion Science* (Sherman, P. ,editor), Academic Press, London, New York.

[14] Robinson D. A. and S. P. Friedman (2001). The effect of particle size distribution on the effective dielectric permittivity of saturated granular media, *Water Resour. Res.*, *37,* 33-40.

[15] Robinson D. A. and S. P. Friedman (2002). The effective permittivity of dense packings of glass beads, quartz sand and their mixtures immersed in different dielectric backgrounds, *J. Non-Crystalline Solids*, *305*, 261-267.

[16] Robinson D. A. and S. P. Friedman (2003). A method for measuring the solid particle permittivity of rocks, sediments and granular materials, *J.Geophys. Res.*, 108(B2), 2075, doi:10.1029/2001JB000691.

[17] Birchack J.R., C.Z.G. Gardner, J.E. Hipp and J.M. Victor (1974). High dielectric constant microwave probes for sensing soil moisture, *Proc. IEEE*, *62*, 93-98, 1974.

[18] Whalley, W. R. (1993). Considerations on the use of time-domain reflectometry (TDR) for measuring soil water content, *J. Soil Sci.*, *44*, 1-9.

[19] Sihvola, A., and J. A. Kong (1988). Effective permittivity of dielectric mixtures, *IEEE Trans. Geosci. Remote Sens., 26*, 420-429.

[20] Sihvola, A., and J. A. Kong (1989). Correction to "Effective permittivity of dielectric mixtures," *IEEE Trans. Geosci. Remote Sens., 21*, 101-102.

[21] Sen P.N., C. Scala and M.H. Cohen (1981). A self-similar model for sedimentary rocks with application to the dielectric constant of fused glass beads. *Geophysics* 46: 5 p. 781-795.

[22] Friedman, S. P., and D. A. Robinson (2002). Particle shape characterization using angle of repose measurements for predicting the effective permittivity and electrical conductivity of saturated granular media, *Water Resour. Res.*, *38*, 10.1029/2001WR000746.

[23] Robinson D.A., and Friedman S. P. (2005) Electrical conductivity and dielectric permittivity of sphere packing: measurements and modelling of cubic lattices, randomly packed monosize spheres and multi-size mixtures. *Physica A. Statistical Mechanics and its Application.,* 358:447-465.

[24] Sareni, B., L. Krähenbühl, A. Beroual, and C. Brosseau (1997). Effective dielectric constant of random composite materials, *J. Appl. Phys.*, *81*, 2375-2383.

[25] Jones S. B. and S. P. Friedman (2000) Particle shape effects on the effective permittivity of anisotropic or isotropic media consisting of aligned or randomly oriented ellipsoidal particles. *Water Resour. Res*., *36,* 2821-2833.

[26] Dafalias, Y. F., and K. Arulanandan (1979). Electrical characterization of transversely isotropic sands, *Arch. Mech.*, *31*, 723-739.

[27] Arulanandan, K. (1991) Dielectric method for prediction of porosity of saturated soil, *J. Geotech. Eng.*, *117*, 319-330.

[28] Thevanayagam, S. (1993). Electrical response of two-phase soil: Theory and applications, *J. Geothech. Eng.*, *119*, 1250-1275.

[29] Friedman, S. P., and S. B. Jones (2001) Measurement and approximate critical path analysis of the pore scale-induced anisotropy factor of an unsaturated porous medium, *Water Resour. Res., 37*, 2929-2942.

[30] Guyon, E., L. Oger, and T. J. Plona (1987). Transport properties in sintered porous media composed of two particles sizes, *J. Phys. D. Appl. Phys.*, *20*, 1637-1644.

[31] Robinson D.A. (2004). Measurement of the solid dielectric permittivity of clay minerals and granular samples using a TDR immersion method. *Vadose Zone Journal* 3 (2): 705-713.

[32] Miyamoto, T., Annaka, T., and J., Chikushi (2005). Extended dual composite sphere model for determining dielectric permittivity of andisols. *Soil Sci. Soc. Am. J,.* 69: 23-29.

[33] Blonquist Jr., J.M., S. B. Jones, I. Lebron, and D. A. Robinson (2006). On the micro-structural and phase configuration effects determining the water content-dielectric relationship of aggregated media, *Water Resources Research*, in press.

[34] Friedman S. P. (2005). Soil properties influencing apparent electrical conductivity: a review. *Computers and Electronics in Agriculture*, 46:45-70.

[35] Thorp, J. M. (1959). The dielectric behaviour of vapours adsorbed on porous solids, *Trans. Faraday Soc.*, *55*, 442-454.

[36] Bockris J.O'M., M.A.V. Devanathan and K. Muller (1963). On the structure of charged interfaces. *Proc. Roy. Soc. London, Ser. A*, *274*, 55-79.

[37] Robinson, D. A., J. D. Cooper, and C. M. K. Gardner (2002). Modeling the relative permittivity of soil hygroscopic water content, *J. Hydrol.*, *255*, 39-49.

[38] Debye, P. (1929). *Polar Molecules*, Dover, New York.

[39] Grant, E. H. (1957). Relationship between relaxation time and viscosity for water, *J. Chem. Phys.*, *26*, 1575-1577.

[40] Kaatze, U. (1996). Microwave dielectric properties of water, Chapter 2, pp. 37-53, in *Microwave Aquametry Electromagnetic wave interaction with water-containing materials*. (Editor A. W. Kraszewski.) IEEE Press, Piscataway, NJ.

[41] Low, P. F. (1976). Viscosity of interlayer water in montmorillonite, *Soil Sci. Soc. Am. J.*, *40*, 500-505.

[42] McBride, M. B., and P. Baveye (1995). Mobility of anion spin probes in hectorite gels: viscosity of surficial water, *Soil Sci. Soc. Am. J.*, *59*, 388-394.

[43] Or, D., and J.M. Wraith (1999). Temperature effects on soil bulk dielectric permittivity measured by time domain reflectometry: A physical model, *Water Resour. Res.*, 35*,* 371-383.

[44] Sposito, G., and R. Prost (1982). Structure of water adsorbed on smectites, *Chem. Rev., 82*, 553-573.

[45] Hilhorst, M. A., C. Dirksen, F. W. H. Kampers, and R. A. Feddes (2001). Dielectric relaxation of bound water versus soil matric pressure, *Soil Sci. Soc. Am. J.*, *65*, 311-314.

[46] Hoekstra, P., and A. Delaney (1974). Dielectric properties of soil at UHF and microwave frequencies, *J. Geophys. Res.*, *79*, 1699-1708.

[47] Friel, R., and D. Or (1999). Frequency analysis of time-domain reflectometry (TDR) with application to dielectric spectroscopy of soil constituents, *Geophys.*, *64*, 1-12.

[48] Shang, J. Q., R. K. Rowe, J. A. Umana, and J. W. Scholte (1999). A complex permittivity measurement system for undisturbed/compacted soils, *Geotechnical Testing J.*, *22*, 165-174.

[49] Cosenza, P., C. Camerlynck, and A. Tabbagh (2003). Differential effective medium schemes for investigating the relationship between HF relative dielectric permittivity and water content of soils, *Water Resour. Res., 39*, 1230, doi:10.1029/2002WR001774.

[50] Sihvola, A. and I.V. Lindell (1990). Polarizability and effective permittivity of layered and continuously inhomogeneous dielectric ellipsoids, *J. Elec. Waves Appl.*, *4*, 1-26.

[51] Li, C. B., A. Zhao, and S. P. Friedman (2005). A new method to evaluate adsorption energies between cations and soil particles via Wien effect measurements in dilute suspensions. *Environ Science and Technology*, 39*:*6757-6764. doi:10.1021/es050070b.

[52] Henderson, D (1983). Recent progress in the theory of the electric double layer. *Progress in Surface Science*, 13:197-224.

[53] Pottel, R. (1973). Dielectric properties, in "*the Physics and Physical Chemistry of Water: A Comprehensive Treatise",* Franks, F. (Ed.), Vol. 3, Chap. 8, pp. 401-431, Plenum Press, New York.

[54] Chen, Y., and D. Or (2006). Geometrical factors and interfacial processes affecting complex dielectric permittivity of partially saturated porous media, submitted to *Water Resources Research*.

Biographical Information

Shmulik P. Friedman obtained a B.Sc. degree and a Ph.D. in Agriculture from the Hebrew University of Jerusalem. He is a research scientist and currently the head of the department of environmental physics and irrigation in the Institute of Soil, Water and Environmental Sciences of the Agricultural Research Organization, Bet Dagan, Israel.

Scott B. Jones obtained a B.Sc. degree from Brigham Young University in Civil Engineering and from Utah State University he received an M.S. in Agricultural and Irrigation Engineering and a Ph.D. in Soil Physics. He is currently an assistant professor of soil physics at Utah State University in Logan, Utah.

David A. Robinson obtained a B.Sc. degree from Reading University U.K. in Soil Science with Sedimentary Geology and a Ph.D. in Soil Hydrology conducted at the Institute of Hydrology and University of Ulster U.K. He is currently a program officer at Stanford University, working with the Consortium of Universities for the Advancement of Hydrologic Sciences Inc (CUAHSI) as the Operations Director of the Hydrologic Measurement Facility (HMF), Stanford, California.